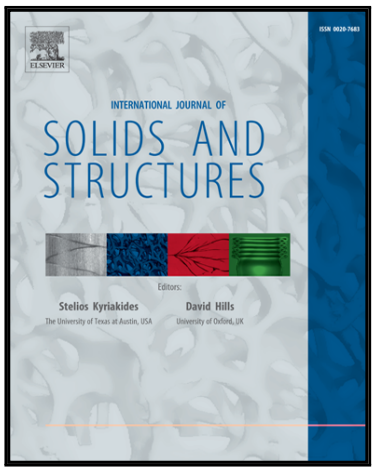

Multiscale Structural Analysis of Textile Composites Using Mechanics of Structure Genome

Khizar Rouf, Xin Liu, Wenbin Yu

PII: S0020-7683(17)30540-1
DOI: 10.1016/j.ijsolstr.2017.12.005
Reference: SAS 9823

To appear in: *International Journal of Solids and Structures*

Received date: 7 June 2017
Revised date: 21 November 2017
Accepted date: 6 December 2017

Please cite this article as: Khizar Rouf, Xin Liu, Wenbin Yu, Multiscale Structural Analysis of Textile Composites Using Mechanics of Structure Genome, *International Journal of Solids and Structures* (2017), doi: 10.1016/j.ijsolstr.2017.12.005

Multiscale Structural Analysis of Textile Composites Using Mechanics of Structure Genome

Khizar Rouf, Xin Liu, Wenbin Yu

School of Aeronautics and Astronautics, Purdue University, West Lafayette, IN, USA, 47907-2045

Abstract

Mechanics of structure genome (MSG) is used to develop an approach for multiscale structural analysis of textile structures. First, MSG is used to predict the properties of yarns having realistic geometry. Then, beam and plate stiffness matrices are predicted based on the yarn and matrix properties using MSG. These beam and plate stiffness matrices are used to perform structural analysis of textile beams and plates. The computed global responses are used to conduct dehomogenization to obtain local stress fields. The MSG-based global displacement and local stress fields are compared with those predicted by direct numerical simulation (DNS) to compare accuracy and computational efficiency. An excellent agreement was observed for both global displacement and local stress field results, while the computational cost and modeling effort of MSG-based analysis are significantly lower than those of DNS.

Keywords:

Structure genome, Multiscale structural analysis, Textile composites

Email address: liu1512@purdue.edu (Xin Liu)

Nomenclature

$[\boldsymbol{C}^b]_{4\times4}$	Beam stiffness matrix for the Euler-Bernoulli beam model
$[\boldsymbol{C}]_{6\times6}$	Material stiffness matrix
$\boldsymbol{A}, \boldsymbol{B}, \boldsymbol{D}$	Plate stiffness matrix for the Kirchhoff-Love plate model
σ_{ij}	Stress field
ε_{ij}	Strain field
F_1, M_i	Beam stress resultants
$N_{\alpha\beta}, M_{\alpha\beta}$	Plate stress resultants
U_{1D}	Strain energy density for the beam model
U_{2D}	Strain energy density for the plate model
w_i	Fluctuating functions
x_i	Macro-coordinates for the structure
y_i	Micro-coordinates for the structure genome

1. Introduction

Textile composites have gained technological importance in structural applications because of their potential benefits. These composites not only possess the advantages of low weight to in-plane stiffness ratio like unidirectional composites, but also offer better out-of-plane properties. Two-dimensional (2D) textile composites such as woven fabric composites (WFCs) and braided composites exhibit better through-the-thickness properties because of yarn interlacement. In addition to that, 2D textile composites provide balanced

in-plane properties, unlike unidirectional composites where one direction is much stiffer than the other two directions. Three-dimensional (3D) textile composites are even more beneficial because they have reinforcement in multiple directions. Therefore, they have higher fracture toughness and impact resistance as compared to laminated composites which are prone to delamination [1]. Another major advantage of 3D woven composites is to fabricate structural component preforms directly from the yarns. It enables manufacturing of complicated structural parts without using fasteners, thus reduces the manufacturing costs significantly. An example of such applications is I-beams made by 3D weaving [2].

Utilization of textile composites in structural applications requires an accurate and efficient structural analysis. A key requirement in the accurate prediction of structural behavior is to use correct constitutive relation of textile composites. The elastic properties of textile composites are usually predicted by a two-step homogenization approach [3, 4]. In the first step, the effective elastic properties of yarn are obtained from constituent material properties. A common practice is 3D representative volume element (RVE) analysis to predict 3D properties of yarn. This approach is computationally expensive and requires significant modeling efforts particularly when a periodic mesh is necessary for imposing periodic boundary conditions (PBCs). Furthermore, RVE usually has a cuboidal shape while a realistic modeling of yarns may require a representation of the entire yarn which has curved boundary surfaces.

The second homogenization stage usually deals with determining the effective properties of textile composites from the yarn and matrix properties

[5]. Many real composite structures are thin or slender structural components which might be made by textile composites such as I-beams, skin panels, wing-cover panels, stitched stiffeners etc. Engineers usually use shell or beam elements to analyze this kind of textile composite structures. However, there are not many models available to predict the equivalent beam and plate stiffness for textile composites that can be used directly for the macroscopic structural analysis.

For beam-like textile structures, [6] proposed a finite element analysis (FEA) based model to predict the beam stiffness matrix. In this analysis, they implemented PBCs on the lateral faces of unit cell, while top and bottom surfaces were assumed traction free. They applied three independent deformations (pure extension, pure bending, and pure shear) to predict the beam stiffness coefficients. The predicted results for plain weave textile were compared with the estimated results from a mosaic model, and a good agreement was found.

For plate-like textile structures, some researchers have attempted to predict plate stiffness matrices using different approaches. Most of these predictions are based on the classical laminated plate theory (CLPT). For 2D woven textiles, [7, 8, 9] conducted earlier analytical predictions using CLPT. In these predictions, 2D woven composites were modeled in series and parallel based on the loading direction. [10] proposed a fiber inclination model based on CLPT to predict equivalent plate stiffness for 3D textile composites, which agrees reasonably well with experiments for 3D braided composites. [11] developed another analytical model based on CLPT to determine the plate stiffness of twill composites. The predicted results compared well with

experiments. [12] developed a direct FEA based micromechanics model with the main focus to predict plate stiffness. That model was applied to plain weave composites and satin weave composites, and the predicted results were compared with those predicted by a mosaic model and CLPT. Many other researchers have attempted to predict 3D elastic properties of 2D and 3D textiles which are based on different assumptions such as iso-strain, iso-stress, mixed iso-strain and iso-stress. Besides the loss of accuracy due to the associated assumptions in the derivations of 3D elastic properties, [12] have pointed out that textile plate stiffness matrices, especially B and D matrices, cannot be predicted using the homogenized elastic constants and plate thickness in conjunction with CLPT. Therefore, plate stiffness properties should be predicted directly in terms of the textile microstructures.

Based on the literature review, there are several issues with the available models for predicting the beam and plate stiffness matrices. First, most models are based on some assumptions which might affect the accuracy. Some assumptions are made for defining the kinematics, and others for the yarn path. Second, models are usually applicable to some specific textile microstructures due to the associated assumptions for describing the complex microstructure. A unified approach that can handle general textile microstructures will be of great value for answering design questions related with different woven architectures. Third, few plate and beam models can accurately predict the local stress and strain fields which are important for the failure analysis of textile structures. Therefore, it is the objective of this paper to use MSG, a formal framework for multiscale constitutive modeling proposed by Yu [13] to develop an efficient yet accurate multiscale analysis for

beams and plates made with general textile composites. MSG has the possibility to predict structural properties in terms of microstructures without unnecessary scale separation. MSG is based on the principle of minimum information loss (PMIL) to minimize the information loss between the original model and the homogenized model. It has already been shown that MSG has the capability to efficiently and accurately analyze composite beams, composite plates, and other composite structures [14, 15, 16, 17]. It can also be used to perform the two-step homogenization of textile composites for predicting effective 3D properties of textile composites [3]. Different from the previous MSG papers, effective yarn properties will be predicted considering the realistic cross section shape in this paper. Besides, we will extend MSG to construct beam models and plate models for textile structures to compute equivalent beam/plate properties in terms of woven microstructures. Unlike the plate and beam problems solved in other MSG papers [14, 15, 16, 17], textile beam and plate problems have some unique features. First, due to the 3D heterogeneity of woven composites, 3D SGs must be used at the macro-homogenization step. Second, the local material orientations change along the yarn path in the woven SGs, and the MSG beam and plate models have been extended to consider this important feature.

The corresponding theory has been implemented in SwiftComp$^{\text{TM}}$, a general-purpose multiscale constitutive modeling software. It takes the geometric model and material properties of a SG and computes the constitutive properties for the macroscopic structural analysis in the form of beam stiffness matrix, plate stiffness matrix, or 3D properties. We have also integrated SwiftComp with TexGen, a powerful geometry model generator for textile

composites [18]. Various examples are used to demonstrate the application of the present approach. Both the global displacements and local stresses using the present approach are compared with direct numerical simulations (DNS) to evaluate the accuracy and efficiency of MSG-based multiscale structural analysis of textile composites.

2. MSG for multiscale modeling of textile structures

2.1. MSG-based beam and plate modeling

This section extends MSG to construct beam and plate models for textile composites. Although MSG can be applied to geometrically nonlinear and material nonlinear problems, we will only deal with linear elastic behavior governed by the 3D linear elasticity which is formulated in terms of 3D displacements, u_i, strains, ε_{ij}, stresses, σ_{ij}, and Hooke's law. In MSG, we need to introduce two sets of coordinates including macro-coordinates x_i and micro-coordinates y_i. The original structure is described using the macro-coordinates x_i. Depending on the dimensionality of the macroscopic structural model, some of the macro-coordinates will be eliminated. For beam-like structures, field measures of a beam model are represented as functions of x_1 defined along the beam reference line, while x_2 and x_3 are eliminated as shown in Figure 1c. For plate-like structures, field measures of a plate model are represented as a function of x_1 and x_2 defined over the reference surface, while x_3 is eliminated as shown in Figure 2c. We also use micro-coordinates $y_i = x_i/\varepsilon$ to describe the SG with ε being a small parameter due to the fact that the microscopic size of the SG is much smaller than the macroscopic size of the structure. In multiscale structural modeling, a field function of the

original heterogeneous structure can be generally written as a function of the macro-coordinates x_k which remain in the macroscopic structural model and the micro-coordinates y_j. Following [19], the partial derivative of a function $f(x_k, y_j)$ can be expressed as

$$\frac{\partial f(x_k, y_j)}{\partial x_i} = \frac{\partial f(x_k, y_j)}{\partial x_i}|_{y_j=\text{const}} + \frac{1}{\varepsilon}\frac{\partial f(x_k, y_j)}{\partial y_i}|_{x_k=\text{const}} \equiv f_{,i} + \frac{1}{\varepsilon}f_{|i} \quad (1)$$

2.1.1. MSG-based Euler-Bernoulli beam model

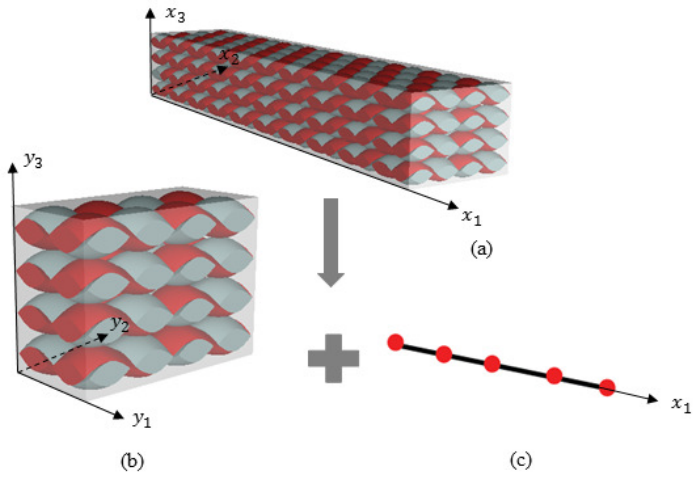

Figure 1. Beam SG and 1D beam analysis for a beam-like textile structure: a) 3D textile structure; b) 3D SG; c) 1D beam elements

To derive the Euler-Bernoulli beam model using MSG, we need to first express the 3D displacement field of the original structure in terms of that of the Euler-Bernoulli beam model [13]:

$$\begin{aligned} u_1(x_1, y_1, y_2, y_3) &= \overline{u}_1(x_1) - \varepsilon y_2 \overline{u}_2'(x_1) - \varepsilon y_3 \overline{u}_3'(x_1) + \varepsilon w_1(x_1, y_1, y_2, y_3) \\ u_2(x_1, y_1, y_2, y_3) &= \overline{u}_2(x_1) - \varepsilon y_3 \Phi_1(x_1) + \varepsilon w_2(x_1, y_1, y_2, y_3) \\ u_3(x_1, y_1, y_2, y_3) &= \overline{u}_3(x_1) + \varepsilon y_2 \Phi_1(x_1) + \varepsilon w_3(x_1, y_1, y_2, y_3) \end{aligned} \quad (2)$$

where u_i and $\overline{u}_i$ denote the displacements of the original 3D heterogeneous structure and the 1D beam model respectively. Beam displacements are only functions of x_1. Φ_1 is the sectional rotation. w_1, w_2 and w_3 are the unknown fluctuating functions, which are used to describe the differences between the the homogenized model and the original heterogeneous model in displacement fields. We can choose the constraints for the unknown fluctuating functions as [13]

$$\langle w_i \rangle = 0; \;\; \langle w_{3|2} - w_{2|3} \rangle = 0 \tag{3}$$

where the angle bracket "$\langle \cdot \rangle$" denotes the integration over the SG, the 3D volume in Figure 1b. Note Eq. (3) represents four constraints because "i" is a free index. In this formulation, there are no apriori assumptions about the kinematics such as the commonly invoked Euler-Bernoulli assumptions. The introduction of the fluctuating functions enables to describe all the possible displacements of every material point of a beam-like structure made of textile composites, which cannot be adequately expressed by the simple kinematics of the Euler-Bernoulli model.

The infinitesimal strain field in the 3D linear elasticity theory can be defined as:

$$\varepsilon_{ij} = \frac{1}{2}(\frac{\partial u_i}{\partial x_j} + \frac{\partial u_j}{\partial x_i}) \tag{4}$$

Plugging Eq. (2) into Eq. (4), and drop the asymptotically smaller terms based on variational asymptotic method (VAM) [20]. The 3D strain field can

be expressed as:

$$\begin{aligned}
\varepsilon_{11} &= \epsilon_1 + \varepsilon y_3 \kappa_2 - \varepsilon y_2 \kappa_3 + w_{1|1} \\
\varepsilon_{22} &= w_{2|2} \\
\varepsilon_{33} &= w_{3|3} \\
2\varepsilon_{12} &= w_{1|2} - \varepsilon y_3 \kappa_1 + w_{2|1} \\
2\varepsilon_{13} &= w_{1|3} + \varepsilon y_2 \kappa_1 + w_{3|1} \\
2\varepsilon_{23} &= w_{2|3} + w_{3|2}
\end{aligned} \tag{5}$$

Here, the strain measures for the beam model are defined as:

$$\epsilon_1 = \overline{u}_1'; \ \kappa_1 = \Phi_1'; \ \kappa_2 = -\overline{u}_3''; \ \kappa_3 = \overline{u}_2'' \tag{6}$$

where ϵ_1 is the extensional strain, κ_1 is the twist rate, κ_2 and κ_3 are the beam bending curvatures about the x_2 and x_3 axes respectively. The $(')$ denotes the derivative with respect to x_1.

The strain energy density for a beam model can be defined as:

$$U_{1D} = \frac{1}{2}\langle \sigma_{ij}\varepsilon_{ij} \rangle = \frac{1}{2}\langle C_{ijkl}\varepsilon_{ij}\varepsilon_{kl} \rangle \tag{7}$$

where σ_{ij} is the stress field which is related to ε_{ij} according to Hooke's law.

$$\sigma_{ij} = C_{ijkl}\varepsilon_{kl} \tag{8}$$

It is noted that C_{ijkl} could be pointwisely varying because of the heterogeneity due to fiber, yarn, matrix and continously varying yarn orientations.

In this paper, we focus on the static behavior and the kinetic energy is neglected. The total potential energy of the original 3D structure can be defined as:

$$\Pi = \frac{1}{2}\int_0^L U_{1D} dx_1 - W \tag{9}$$

where W is the work done by external sources. Substitute the 3D strain field in Eq. (5) into the total potential energy in Eq. (9) and drop small terms according to the VAM. Minimize potential energy and impose the constraints in Eq. (3), the fluctuating functions, w_i, can be determined. Substitute the obtained fluctuating functions back into Eq. (5), the 3D strain field can be expressed in terms of 1D beam strain measures defined in Eq. (6). Substituting the 3D strain field into Eq. (7), one obtains the 1D beam strain energy density.

The 1D kinetic variables, commonly called sectional resultants, can be defined as the conjugates of beam strains:

$$\begin{aligned} \frac{\partial U_{1D}}{\partial \epsilon_1} &= F_1; \quad \frac{\partial U_{1D}}{\partial \kappa_1} = M_1 \\ \frac{\partial U_{1D}}{\partial \kappa_2} &= M_2; \quad \frac{\partial U_{1D}}{\partial \kappa_3} = M_3 \end{aligned} \tag{10}$$

The sectional resultants can be related with beam strains through the beam stiffness matrix as follows:

$$\begin{Bmatrix} F_1 \\ M_1 \\ M_2 \\ M_3 \end{Bmatrix} = \begin{bmatrix} C^b_{11} & C^b_{12} & C^b_{13} & C^b_{14} \\ C^b_{12} & C^b_{22} & C^b_{23} & C^b_{24} \\ C^b_{13} & C^b_{23} & C^b_{33} & C^b_{34} \\ C^b_{14} & C^b_{24} & C^b_{34} & C^b_{44} \end{bmatrix} \begin{Bmatrix} \epsilon_1 \\ \kappa_1 \\ \kappa_2 \\ \kappa_3 \end{Bmatrix} \tag{11}$$

Here, the beam stiffness matrix $\boldsymbol{C^b}$ could be a fully populated 4×4 matrix for the Euler-Bernoulli beam model, and the superscript "b" indicts the stiffness matrix is for the beam model which is different from the material stiffness matrix. Note the elements of the beam stiffness matrix cannot be explicit written as material parameters and geometry parameters such as EA for conventional beam theory for isotropic homogeneous beams. This stiffness

matrix can be used as input to conduct the macroscopic beam analysis, which will compute the beam strain measures $\{\epsilon_1, \kappa_1, \kappa_2, \kappa_3\}$. The beam analysis remains the same as those in [14]. For simple beam problems like a cantilever beam, the beam analysis can be solved using the knowledge from undergraduate strength of materials, which is given in section 4.1. Plugging the beam strain measures back into Eq. (5), the local 3D strain field can be obtained through dehomogenization. Using Hook's law, the local stress field can be obtained. The formulas for computing the beam stiffness matrix and dehomogenization can be found in the Appendix A.

2.1.2. MSG-based Kirchhoff-Love plate model

To derive the Kirchhoff-Love plate model using MSG, the 3D displacement field can be expressed in terms of the 2D displacement variables admitted by the Kirchhoff-Love plate model as [13]:

$$\begin{aligned} u_1(x_1, x_2, y_1, y_2, y_3) &= \overline{u}_1(x_1, x_2) - \varepsilon y_3 \overline{u}_{3,1}(x_1, x_2) + \varepsilon w_1(x_1, x_2, y_1, y_2, y_3) \\ u_2(x_1, x_2, y_1, y_2, y_3) &= \overline{u}_2(x_1, x_2) - \varepsilon y_3 \overline{u}_{3,2}(x_1, x_2) + \varepsilon w_2(x_1, x_2, y_1, y_2, y_3) \\ u_3(x_1, x_2, y_1, y_2, y_3) &= \overline{u}_3(x_1, x_2) + \varepsilon w_3(x_1, x_2, y_1, y_2, y_3) \end{aligned} \tag{12}$$

where u_i and $\overline{u}_i$ denote the displacements of the original 3D heterogeneous structure and the 2D plate model respectively. Plate displacements are functions of x_1 and x_2. w_1, w_2, and w_3 are the unknown fluctuating functions. In this formulation, there are no apriori assumptions about the kinematics such as the commonly invoked Kirchhoff-Love assumptions. The introduction of the fluctuating functions enables to describe all the possible displacements for every material point of a plate-like structure made of textile composites, which cannot be adequately expressed by the simple kinematics of the

Kirchhoff-Love model.

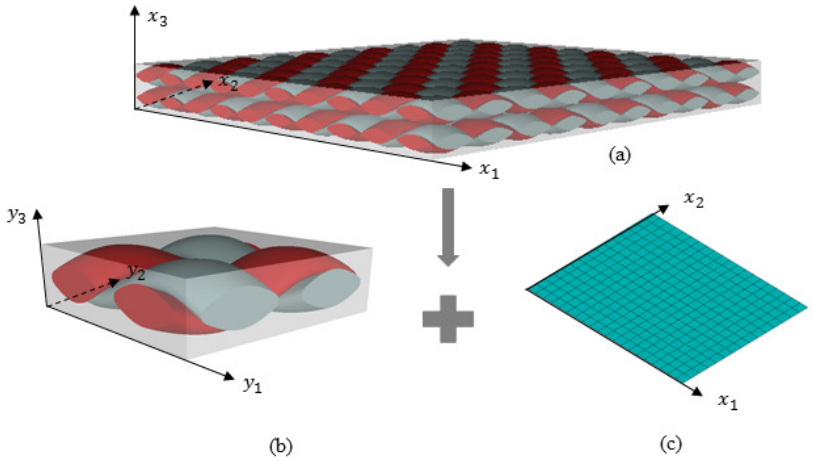

Figure 2. SG and 2D analysis for a plate-like textile structure: a) 3D textile structure; b) 3D SG; c) 2D plate elements

Based on Eq. (4), and drop the asymptotically small terms based on VAM. The 3D strain field can be written as:

$$\begin{aligned}
\varepsilon_{11} &= \epsilon_{11} + \varepsilon y_3 \kappa_{11} + w_{1|1} \\
\varepsilon_{22} &= \epsilon_{22} + \varepsilon y_3 \kappa_{22} + w_{2|2} \\
\varepsilon_{33} &= w_{3|3} \\
2\varepsilon_{12} &= 2\epsilon_{12} + 2\varepsilon y_3 \kappa_{12} + w_{1|2} + w_{2|1} \\
2\varepsilon_{13} &= w_{1|3} + w_{3|1} \\
2\varepsilon_{23} &= w_{2|3} + w_{3|2}
\end{aligned} \tag{13}$$

where the plate strains and curvatures are defined as:

$$\epsilon_{\alpha\beta}(x_1, x_2) = \frac{1}{2}(\overline{u}_{\alpha,\beta} + \overline{u}_{\beta,\alpha}); \ \kappa_{\alpha\beta}(x_1, x_2) = -\overline{u}_{3,\alpha\beta} \tag{14}$$

The total potential energy of the 3D structure can be defined as:

$$\Pi = \frac{1}{2}\int_s U_{2D} ds - W \tag{15}$$

where U_{2D} is the 2D strain energy density defined as:

$$U_{2D} = \frac{1}{2}\langle \sigma_{ij}\varepsilon_{ij}\rangle = \frac{1}{2}\langle C_{ijkl}\varepsilon_{ij}\varepsilon_{kl}\rangle \tag{16}$$

Following the same procedure as for MSG-based beam model with the fluctuating functions constrained by:

$$\langle w_i \rangle = 0 \tag{17}$$

Drop the small terms according to VAM and minimize the potential energy. Impose the constraints for fluctuating functions to solve for w_i. Substitute the obtained fluctuating functions back into Eq. (13). The 3D strain field can be expressed in terms of 2D plate strains and curvatures in Eq. (14).

The 2D kinetic variables called plate stress resultants are defined as:

$$\begin{gathered}\frac{\partial U_{2D}}{\partial \epsilon_{11}} = N_{11};\ \frac{\partial U_{2D}}{\partial 2\epsilon_{12}} = N_{12};\ \frac{\partial U_{2D}}{\partial \epsilon_{22}} = N_{22} \\ \frac{\partial U_{2D}}{\partial \kappa_{11}} = M_{11};\ \frac{\partial U_{2D}}{\partial 2\kappa_{12}} = M_{12};\ \frac{\partial U_{2D}}{\partial \kappa_{22}} = M_{22}\end{gathered} \tag{18}$$

We can get the plate constitutive relation to relate the plate stress resultants and strains and curvatures as:

$$\begin{Bmatrix} N_{11} \\ N_{22} \\ N_{12} \\ M_{11} \\ M_{22} \\ M_{12} \end{Bmatrix} = \begin{bmatrix} A_{11} & A_{12} & A_{16} & B_{11} & B_{12} & B_{16} \\ A_{12} & A_{22} & A_{26} & B_{12} & B_{22} & B_{26} \\ A_{16} & A_{26} & A_{66} & B_{16} & B_{26} & B_{66} \\ B_{11} & B_{12} & B_{16} & D_{11} & D_{12} & D_{16} \\ B_{12} & B_{22} & B_{26} & D_{12} & D_{22} & D_{26} \\ B_{16} & B_{26} & B_{66} & D_{16} & D_{26} & D_{66} \end{bmatrix} \begin{Bmatrix} \epsilon_{11} \\ \epsilon_{22} \\ 2\epsilon_{12} \\ \kappa_{11} \\ \kappa_{22} \\ 2\kappa_{12} \end{Bmatrix} \tag{19}$$

Here, the 6×6 plate stiffness matrix is composed of the A, B and D matrices needed for the Kirchhoff-Love plate model. Although we used the same notation of A, B, D matrices from CLPT, the way to obtain these stiffness matrices has no relations to that has been used to derive CLPT [13]. The stiffness matrix can be directly used in the shell elements in finite element software packages such as Abaqus and Ansys to conduct the macroscopic plate analysis, which can take a plate stiffness matrix as inputs. Similar to the MSG beam model, the plate strain measures can be obtained from structural analysis, and the local strain field can be computed using Eq. (13). The local stress field can be obtained using Hook's law. The formulas for obtaining the plate stiffness matrix and dehomogenization can be found in the Appendix A.

2.2. MSG-based multiscale modeling framework for textile composites

MSG-based multiscale modeling of textile composite structures can be divided into three steps: homogenization (microscale and macroscale), structural analysis and dehomogenization as shown in Figure 3.

2.2.1. Micro-homogenization

The first step in the multiscale modeling of textile composite structures is to identify SG for yarns. Since yarns exhibit heterogeneity over the cross section of the yarn and uniformity along the yarn path, they can be modeled using a 2D SG as shown in Figure 4b. Although the analysis domain is 2D, the strain energy is still expressed in terms of the 3D strain field. Thus MSG can compute effective properties by using a 2D domain. The microstructure of the yarn is usually idealized in the literature as a square pack or hexagonal

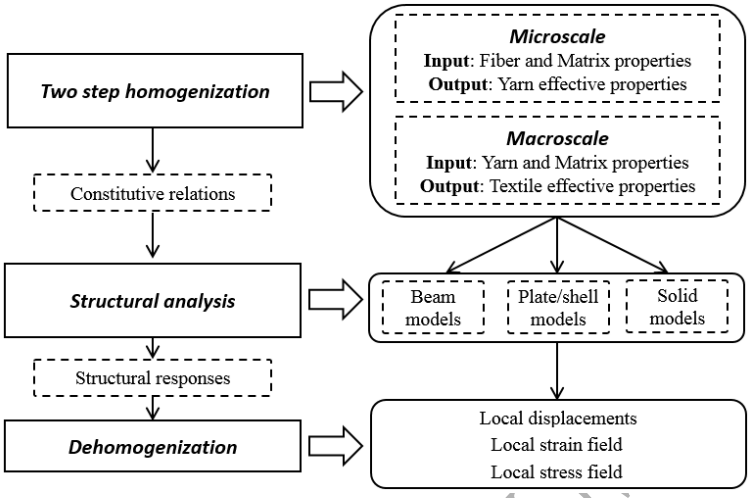

Figure 3. MSG-based modeling framework for textile composites

pack. MSG can also handle a SG for the yarn having multiple fibers with real cross-sectional shape such as an ellipse. For an elliptical shape, aperiodic constraints can be imposed which has been demonstrated as an effective way to consider the non-periodicity feature of a SG [3]. This modeling approach allows analysts to predict 3D properties of hybrid yarns (with more than one fiber type) and to study the effect of varied fiber distribution inside the yarn. Once the yarn properties have been determined, then MSG can be used to determine the beam stiffness matrix, plate stiffness matrix or 3D properties in the macro-homogenization step. In this paper, the homogenized yarn properties are used in Eqs. (7) and (16) to perform macro-homogenization to compute MSG beam and plate stiffness matrices.

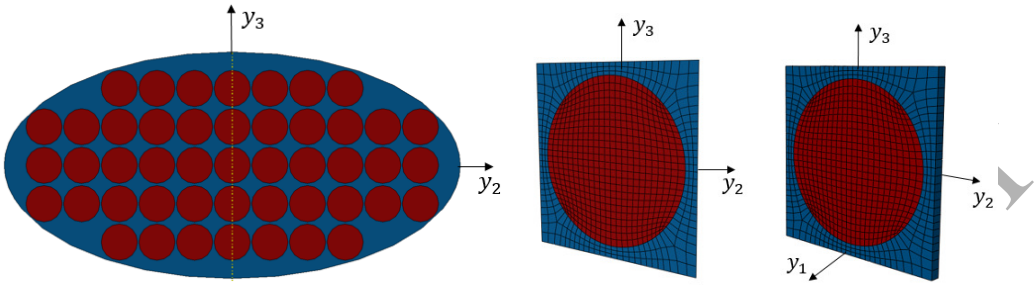

(a) 2D yarn cross-sectional view (b) 2D yarn SG (c) 3D yarn RVE

Figure 4. Three different yarn models

2.2.2. Macro-homogenization for textile composite beams and plates

How to obtain 3D properties in the macro-homogenization for general textile composites considering various effects including finite thickness effects and inter-ply shifts have been presented in [3]. This paper will focus on how to predict effective beam and plate stiffness matrices in the macro-homogenization step. At this level, textile composites exhibit heterogeneity in three dimensions; therefore, a 3D SG is needed for the macro-homogenization. Beam SG is the smallest building block of the beam-like structure; therefore, it should be selected in such a way that it can reconstruct the entire beam structure by repeating it in the spanwise direction as shown in Figure 1 (b). For textile plates, SG should be chosen such that it can reconstruct the entire structure by repeating it in the two in-plane directions. An example of a plate SG is presented in Figure 2 (b). Once the SG has been identified, MSG can be used to predict the constitutive relation for textile beams or plates using the yarn and matrix properties. MSG predicts this constitutive information in the form of beam stiffness matrix or plate stiffness matrix (see Eq. (11) and Eq. (19)). The beam and plate stiffness

matrices can be used as direct inputs for a 1D beam analysis and a 2D plate analysis, respectively.

2.2.3. Dehomogenization

After performing the structural analysis of textile beam or plate like structures, MSG-based dehomogenization analysis can be used to recover the local fields. MSG based dehomogenization is performed over the SG using the global displacements and global strains, which are obtained from the structural analysis. Local strains fields are obtained using Eqs. (5) and (13). These local strain fields are then used with Hook's law to predict the local stresses.

$$\sigma_{ij} = C_{ijlk}\varepsilon_{kl} \tag{20}$$

3. Yarn homogenization

3.1. Yarn homogenization with three approaches

Each yarn, inside a textile composite, contains thousands of randomly packed fibers, which are bonded together through a matrix material. The real yarn cross sections do not have a definite shape, but are often approximated as an ellipse. Due to the irregular shape and random fiber distribution inside the yarn, predicting the yarn properties is a challenge. Therefore, a unit cell, one fiber surrounded by matrix, is commonly used to predict yarn properties. Because MSG has the capability to analyze microstructures with arbitrary shapes, we will use MSG in this section to predict the 3D properties of yarns having different numbers of fibers and realistic shape to verify the validity of the unit cell idealization.

In this section, yarn homogenization is conducted using three different approaches: i) elliptical yarn model with aperiodic boundary conditions (aPBCs), ii) 2D square pack SG model with PBCs, and iii) 3D RVE model with PBCs. For all models, it is assumed that fibers and matrix are perfectly bonded. These models are presented in Figure 4. The constituent properties (carbon fiber (T-300) and epoxy resin-3601) are kept identical across three models, which are taken from [21]. The constituent properties are presented in Table 1.

Table 1. Mechanical properties of the constituents for epoxy 3601/carbon T-300 plain woven composite [21]

Elastic constant	Matrix	Fiber
E_1 (GPa)	4.51	208.80
$E_2 = E_3$ (GPa)	4.51	43.00
$G_{12} = G_{13}$ (GPa)	1.70	7.42
G_{23} (GPa)	1.70	7.42
$\nu_{12} = \nu_{13}$	0.38	0.20
ν_{23}	0.38	0.50

The first homogenization approach deals with modeling yarns with elliptical cross sections. Yarns having different numbers of fibers were modeled using 2D SGs in SwiftComp$^{\text{TM}}$. Nine models having different number of fibers $2, 6, 12, 24, 47, 100$ $200, 300$ and 400 were modeled for homogenization. The minor axis and major axis of ellipse were 8 units $\times$ 3.978 units, and were kept the same across all models. Fiber diameter was changed to maintain fiber volume ratio equal to 60%. Each model was discretized using mixed elements (3-noded triangular elements and 4-noded quadrilateral elements).

The mesh size was 0.025 unit for each model, and then homogenization was conducted by applying aPBCs.

The second MSG-based yarn homogenization approach deals with modeling a 2D SG as shown in Figure 4b. Fiber volume fraction and constituent properties were exactly the same as in the elliptical models. The dimensions of SG were 1 unit $\times$ 1 unit. 2D SG was discretized using 4-noded quadrilateral elements. After meshing, homogenization was carried out by imposing PBCs.

The third approach is 3D RVE analysis of yarn, which was conducted in the commercial software Abaqus 6.13 to compare the elastic constants. The dimensions of RVE were 1 unit $\times$ 1 unit $\times$ 0.05 unit as shown in Figure 4c. The fiber volume ratio and constituent properties were kept the same as in the last two approaches. RVE was discretized using eight-noded hexahedral elements. The mesh size was kept the same in the planar directions as for the 2D SG. The 3D elastic properties were determined by applying PBCs.

3.2. Results and discussion

All nine elastic constants were plotted on log (number of fibers) - linear (elastic constants) scale. From Figure 5a, it can be seen that increasing number of fibers has almost negligible impact on the longitudinal elastic modulus (E_1). This agrees with the earlier finding that fiber distribution has least impact on the longitudinal elastic modulus [22]. However, a different trend was observed for transverse moduli (E_2 and E_3). Transverse moduli values were lower for elliptical models having low number of fibers than the values predicted by 3D RVE and 2D SG models. But, as the number of fibers was increased in the elliptical model, the transverse moduli values increase

towards 3D RVE and 2D SG models-based values as shown in Figure 5b. After modeling 47 fibers in the elliptical model, values of E_2 was converged to that of 3D RVE and 2D SG. However, the values of elliptical model-based E_3 approached to those of 3D RVE and 2D SG after modeling 400 fibers in the elliptical cross section. This implies E_2 converges faster than E_3 in this case because there are more fibers along the y_2 direction.

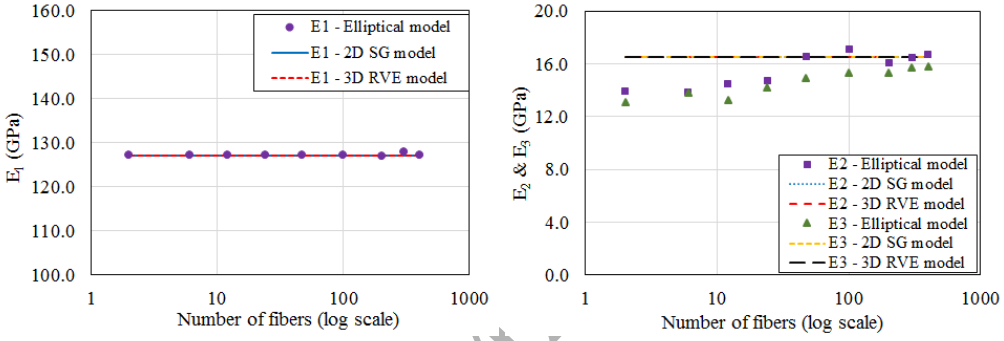

(a) E_1

(b) E_2 and E_3

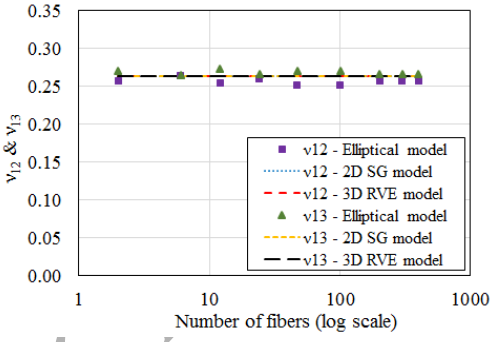

(c) ν_{12} and ν_{13}

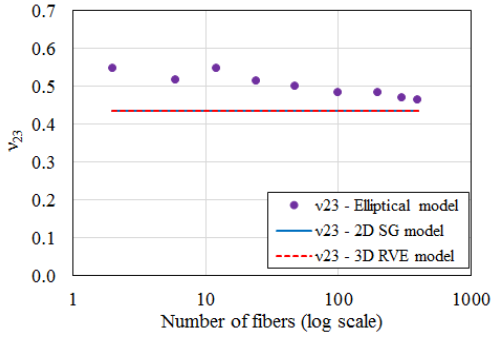

(d) ν_{23}

Figure 5c and 5d present the change in Poisson's ratios (ν_{12}, ν_{13} and ν_{23}) as the number of fibers is increased in the elliptical yarn model. ν_{12} and ν_{13} remains almost insensitive when the number of fibers is increased in the

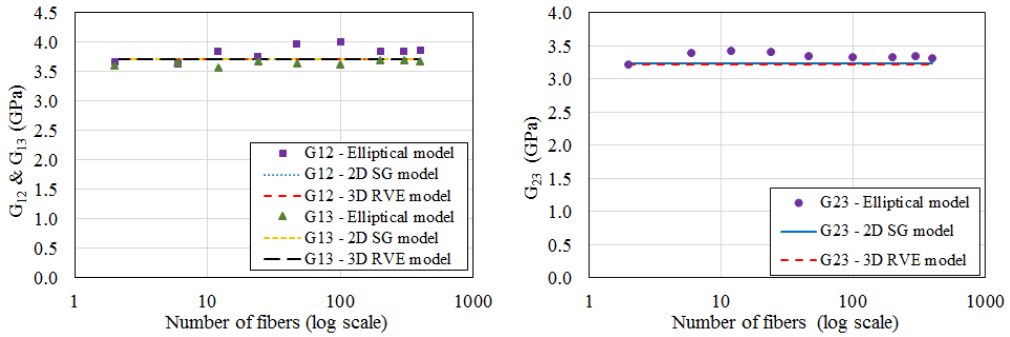

(e) G_{12} and G_{13} (f) G_{23}

Figure 5. Predicted elastic constants

elliptical yarn model. However, the values of ν_{23} changes as the number of fibers is increased. After modeling 400 fibers in the elliptical cross section, the values of ν_{23} approached to those of 2D SG and 3D RVE.

Figure 5e and 5f plots the shear moduli (G_{12}, G_{13} and G_{23}) predicted by 3 three different models. The effect of number of fibers, in the elliptical model, on the shear moduli was found to be negligible. The shear moduli values predicted by three models are in good agreement.

Based on the results obtained by three approaches, the results of 2D SG model show excellent agreement with the results of 3D RVE model. The results of MSG-based elliptical model approaches to the results of the other two models with the increased fibers, which means that MSG-based yarn modeling approach with aPBCs can be used to predict 3D properties of yarns having realistic shapes. This tool can be used to analyze 3D properties of real yarns having multiple fibers inside yarn cross section. On the other hand, it also demonstrates that the idealized unit cell model can be used to predict yarn properties because a real yarn could contain more than 400

fibers.

4. Textile beam and plate analysis

Four textile beam and plate structures were studied to demonstrate accuracy and computational efficiency of MSG-based multiscale structural analysis developed in this paper. For all models, it was assumed that yarns and matrix are perfectly bonded. Further, interface effects at the layer interface were not considered. MSG-based approach for analyzing textile structures follows three steps: homogenization, structural analysis and dehomogenization. The homogenization analyses were implemented in TexGen4SC which can be freely executed on cdmHUB at https://cdmhub.org/tools/texgen4sc. Beam structural analyses were carried out analytically and plate structural analyses were performed using STRI65 element in Abaqus 6.13 with the plate stiffness matrix computed by SwiftComp$^{\text{TM}}$. Both the deflection and local stresses were compared with DNS results.

Deflections and stresses were also predicted using the homogenized 3D material properties, denoted as homogenized approach. For the homogenized approach, the effective material properties were expressed in terms of 6 by 6 material stiffness matrix given in Eq. (21), which was predicted using MSG

for a 3D solid model.

$$\begin{Bmatrix} \sigma_{11} \\ \sigma_{22} \\ \sigma_{33} \\ \sigma_{23} \\ \sigma_{13} \\ \sigma_{12} \end{Bmatrix} = \begin{bmatrix} c_{11} & c_{12} & c_{13} & c_{14} & c_{15} & c_{16} \\ c_{12} & c_{22} & c_{23} & c_{24} & c_{25} & c_{26} \\ c_{13} & c_{23} & c_{33} & c_{34} & c_{35} & c_{36} \\ c_{14} & c_{24} & c_{34} & c_{44} & c_{45} & c_{46} \\ c_{15} & c_{25} & c_{35} & c_{45} & c_{55} & c_{56} \\ c_{16} & c_{26} & c_{36} & c_{46} & c_{56} & c_{66} \end{bmatrix} \begin{Bmatrix} \varepsilon_{11} \\ \varepsilon_{22} \\ \varepsilon_{33} \\ 2\varepsilon_{23} \\ 2\varepsilon_{13} \\ 2\varepsilon_{12} \end{Bmatrix} \tag{21}$$

Although MSG solid model can give accurate predictions for the effective 3D properties of textile composites, but it is not an accurate approach for analyzing slender or thin structures with beam and plate elements. Despite being an inaccurate approach, it is still commonly used in industry to perform textile beam and plate structural analysis using homogenized material properties. We will demonstrate through examples that homogenized approach could cause significant loss of accuracy compared to the MSG beam and plate modelling approach. For beam modeling using the homogenized approach, the material stiffness matrix in Eq. (21) was first input into Abaqus 6.13, then the beam structural analysis using Abaqus is carried out. Since it is difficult to use the beam structural responses for MSG solid dehomogenization, only the stresses at macro-structural level were used to compare with the stresses in other two approaches (MSG and DNS). In other words, because only σ_{11} in the Abaqus beam analysis, only this stress component was compared with the σ_{11} of other two approaches for beam examples. For plate modeling using the homogenized approach, the material stiffness matrix in Eq. (21) is assigned to the shell elements in Abaqus 6.13 to perform plate structural analysis. Like in beam structural analysis using the homogenized

approach, only the stresses at marco-structural level were compared with the stresses in the other two approaches.

For MSG and DNS, only the significant stress components are compared for each example as the other stress components are very small compared to the significant ones. The yarn and matrix properties used in these analyses are presented in Table 2. The matrix properties were taken from [21]. The yarn properties were predicted by 2D SG models from fiber and matrix properties, which have been discussed in the previous section.

Table 2. Predicted elastic constants of real yarn

Parameter	Matrix	Yarn
E_1 (GPa)	4.51	126.91
$E_2 = E_3$ (GPa)	4.51	16.49
$G_{12} = G_{13}$ (GPa)	1.70	3.72
G_{23} (GPa)	1.70	3.22
$\nu_{12} = \nu_{13}$	0.38	0.26
ν_{23}	0.38	0.44

4.1. Analytical solutions for beam responses using MSG beam model

The beam structural responses are solved analytically based on the MSG beam model. The reversed form of Eq. (11) is

$$\begin{Bmatrix} \epsilon_1 \\ \kappa_1 \\ \kappa_2 \\ \kappa_3 \end{Bmatrix} = \begin{bmatrix} S^b_{11} & S^b_{12} & S^b_{13} & S^b_{14} \\ S^b_{12} & S^b_{22} & S^b_{23} & S^b_{24} \\ S^b_{13} & S^b_{23} & S^b_{33} & S^b_{34} \\ S^b_{14} & S^b_{24} & S^b_{34} & S^b_{44} \end{bmatrix} \begin{Bmatrix} F_1 \\ M_1 \\ M_2 \\ M_3 \end{Bmatrix} \tag{22}$$

It is obvious that the $\boldsymbol{S^b}$ matrix in the above equation has the relation with the $\boldsymbol{C^b}$ matrix in Eq. (11) as $\boldsymbol{S^b} = \boldsymbol{C^{b^{-1}}}$. For a beam problem, the beam

stress resultants can be calculated based on the external loading using the knowledge of undergraduate strength of materials. For example, the stress resultants for a cantilever beam subjected to a uniform pressure along negative x_3 direction can be obtained as $M_2 = \frac{1}{2}qx_1^2 - qLx_1 + \frac{1}{2}qL^2$ with F_1, M_1 and M_3 are zeros. q is the uniform pressure and L is the length of the beam. Based on MSG beam model, the beam stiffness matrix has been computed as well as its inversed form in Eq. (22). Then, the beam strain measures can be obtained as $\{\epsilon_1 \quad \kappa_1 \quad \kappa_2 \quad \kappa_3\} = \{S^b_{13}M_2 \quad S^b_{23}M_2 \quad S^b_{33}M_2 \quad S^b_{34}M_2\}$. If the coupling terms S^b_{13}, S^b_{23} and S^b_{34} are zeros, the strain measures become $\kappa_2 = S^b_{33}M_2$ which is just a function of x_1. Using Eq. (6) and the boundary conditions such as $\bar{u}_i(0) = 0$, $\Phi_1(0) = 0$ and $\bar{u}'_2(0) = \bar{u}'_3(0) = 0$ for the cantilever beam, the beam displacements $\bar{u}_i$ and Φ_1 can be computed analytically.

4.2. Plain weave textile beam

This example demonstrates the capability of the present theory for multiscale structural analysis of plain weave textile beam-like structure. This structure consists of two plies of plain weave composite. The length, width and thickness of this structure are 3 mm, 0.3 mm and 0.04 mm respectively. The first step to conduct the MSG-based analysis is to identify the SG of the original structure. 3D SG is used for this beam because plain weave composite has 3D heterogeneity (see Figure 6). The dimensions of the SG are 0.3 mm $\times$ 0.3 mm $\times$ 0.04 mm. The SG was discretized using 86,400 20-noded brick elements.

The non-zero components in the beam stiffness matrix are: $C^b_{11} = 4.49 \times 10^2\,\mathrm{N}$, $C^b_{22} = 1.58 \times 10^{-2}\,\mathrm{N}\cdot\mathrm{mm}^2$, $C^b_{33} = 5.64 \times 10^{-2}\,\mathrm{N}\cdot\mathrm{mm}^2$, $C^b_{44} = 2.96\,\mathrm{N}\cdot$

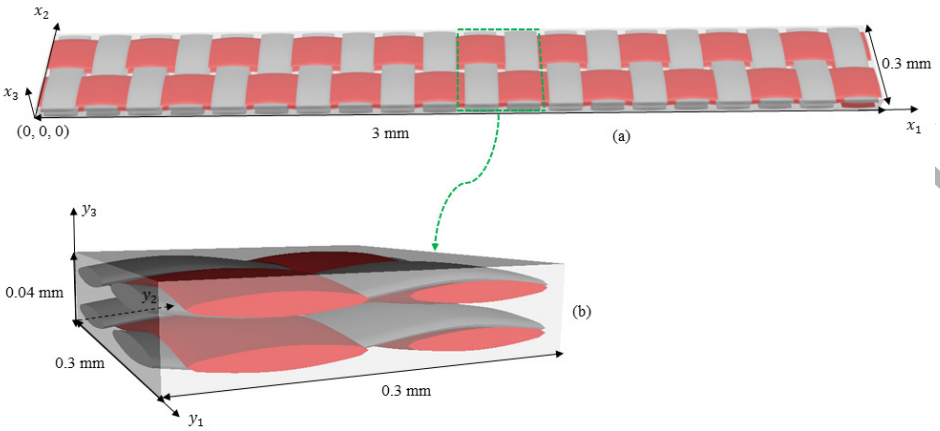

Figure 6. Plain weave composite structure and its SG: a) 3D plain weave structure; b) 3D beam SG

mm^2, $C^b_{14} = C^b_{41} = 2.52 \times 10^{-2}$ N $\cdot$ mm, which were used as inputs for the macroscopic structural analysis. Fixed-free boundary conditions, and the uniform distributed load of magnitude 3×10^{-3} N/mm along negative x_3 direction were used in the computation of the structural responses. In this beam analysis, dehomogenization was performed using the beam strain and curvatures (Eq. (6)) at $x_1 = 1.575$ mm.

To evaluate the efficiency and accuracy of MSG-based multiscale analysis, DNS of the original plain weave beam-like structure was conducted in Abaqus 6.13. The structure was discretized using 864,000 20-noded brick elements.

For the homogenized approach, the non-zero components of the 6×6 material stiffness matrix are: $c_{11} = 4.42 \times 10^4$ N/mm^2, $c_{22} = 4.42 \times 10^4$ N/mm^2, $c_{33} = 1.38 \times 10^4$ N/mm^2, $c_{44} = 2.49 \times 10^3$ N/mm^2, $c_{55} = 2.49 \times 10^3$ N/mm^2, $c_{66} = 2.73 \times 10^3$ N/mm^2, $c_{12} = c_{21} = 7.87 \times 10^3$ N/mm^2, $c_{13} = c_{31} = 6.81 \times 10^3$ N/mm^2, $c_{23} = c_{32} = 6.81 \times 10^3$ N/mm^2. Then the structure is

modelled as a beam made of this homogenized material. It has length 3 mm and cross section with dimensions 0.3 mm $\times$ 0.04 mm. Boundary conditions and load were kept the same as for MSG-based approach.

The displacements for three approaches (MSG, DNS and homogenized) are presented in Figure 7. The results show that MSG-based beam modelling approach predicted beam deflection, $\overline{u}_3$, with almost the same accuracy as DNS. However, the homogenized approach predicted smaller beam deflection as compared to MSG and DNS.

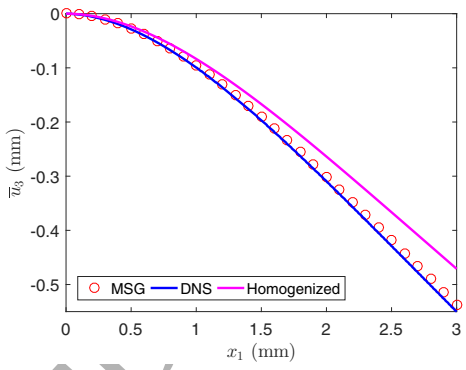

Figure 7. Deflection, $\overline{u}_3$, in plain weave beam along x_1 direction

Figure 8 presents the local stress distribution of σ_{11}, σ_{22} and σ_{33} along the thickness direction. This distribution was taken at $x_1 = 1.575$ mm, $x_2 = 0.075$ mm, $x_3 = 0 - 0.04$ mm. The stress distribution plots show that MSG predictions match excellently with those of DNS. MSG accurately predicted stress distribution through the thickness. In addition to that, the discontinuities in stresses were also captured accurately by MSG. However, the homogenized approach could predict only σ_{11}, and σ_{22} and σ_{33} cannot be recovered from the Abaqus beam analysis. The predicted σ_{11} has linear

stress distribution throughout the thickness which is very different from the exact stress distributions in the original structure predicted by DNS.

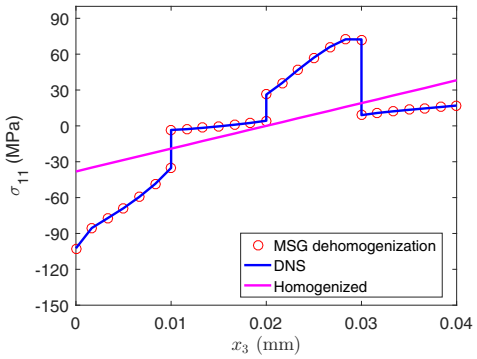

(a) σ_{11}

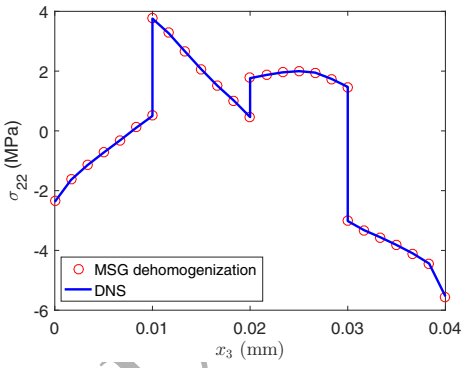

(b) σ_{22}

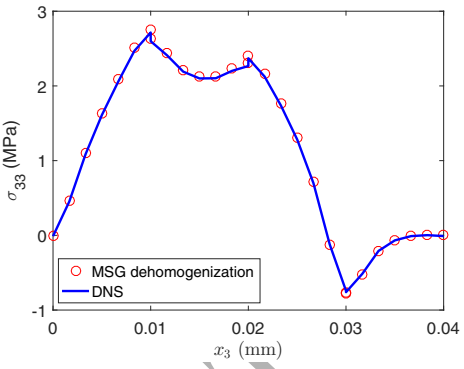

(c) σ_{33}

Figure 8. Stress distribution in plain weave beam through the thickness based on different models

In terms of the computing efficiency, MSG-based beam analysis took approximately two hours and four minutes with one CPU for the entire analysis. However, DNS took seven hours and 44 minutes with 28 CPUs. Based on this analysis, it is clear that MSG can accurately and efficiently analyze plain

weave beam-like textile structures.

4.3. 3D orthogonal textile beam

A 3D orthogonal textile beam structure with more complicated textile architecture is studied in this example. The length, width, and thickness of the original structure are 3 mm, 0.45 mm and 0.07 mm respectively. The original structure and its 3D SG is shown in Figure 9. The dimensions of the SG are 0.3 mm × 0.45 mm × 0.07 mm. SG was discretized using 72,000 20-noded brick elements.

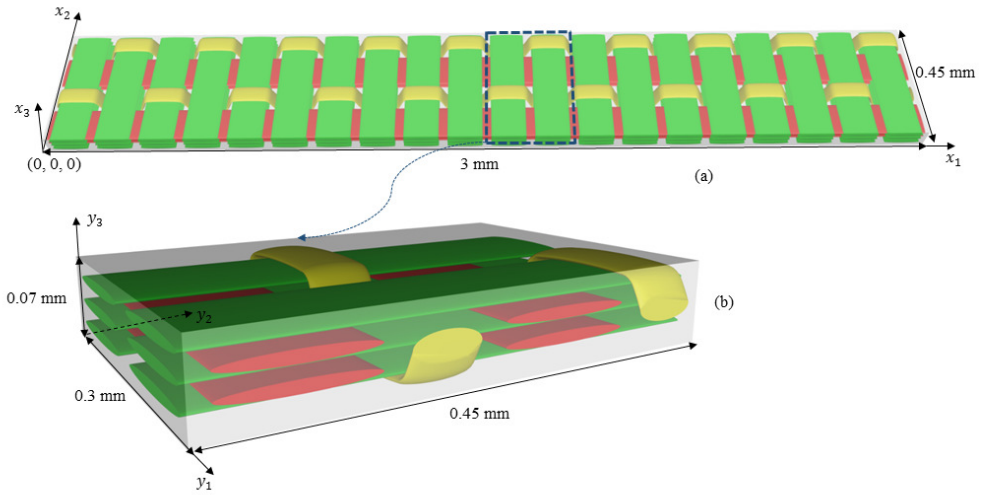

Figure 9. 3D orthogonal composite structure and its SG: a) 3D orthogonal structure; b) 3D beam SG

The non-zero components in the beam stiffness matrix are: $C^b_{11} = 7.12 \times 10^2\,\mathrm{N}$, $C^b_{22} = 9.91 \times 10^{-2}\,\mathrm{N \cdot mm^2}$, $C^b_{33} = 1.52 \times 10^{-1}\,\mathrm{N \cdot mm^2}$, $C^b_{44} = 1.11 \times 10^1\,\mathrm{N \cdot mm^2}$, $C^b_{14} = C^b_{41} = 1.53 \times 10^1\,\mathrm{N \cdot mm}$. Fixed-free boundary conditions

and 4.5×10^{-3} N/mm load along negative x_3 direction were used in the computation of the structural responses. The beam strain and curvatures at $x_1 = 1.575$ mm, were used as inputs for MSG-based dehomogenization analysis and the local fields of the original structure were recovered.

To compare the MSG-based results, DNS of the original 3D orthogonal beam-like structure, presented in Figure 9, was conducted in Abaqus 6.13. 3D orthogonal structure was meshed using 720,000 20-noded brick elements. The boundary conditions and loading were kept the same as for the plain weave beam structure in the previous example.

For the homogenized approach, the non-zero components of the 6×6 material stiffness matrix are: $c_{11} = 2.69 \times 10^4\,\mathrm{N/mm^2}$, $c_{22} = 4.34 \times 10^4\,\mathrm{N/mm^2}$, $c_{33} = 1.17 \times 10^4\,\mathrm{N/mm^2}$, $c_{44} = 2.18 \times 10^3\,\mathrm{N/mm^2}$, $c_{55} = 2.20 \times 10^3\,\mathrm{N/mm^2}$, $c_{66} = 2.42 \times 10^3\,\mathrm{N/mm^2}$, $c_{12} = c_{21} = 6.08 \times 10^3\,\mathrm{N/mm^2}$, $c_{13} = c_{31} = 6.32 \times 10^3\,\mathrm{N/mm^2}$, $c_{23} = c_{32} = 6.00 \times 10^3\,\mathrm{N/mm^2}$. The structure was modelled as a beam made of this homogenized material. It has length 3 mm and cross section with dimensions 0.45 mm $\times$ 0.07 mm. Boundary conditions and load were kept the same as for MSG-based approach.

The displacement field, $\overline{u}_3$, predicted by MSG, DNS, and homogenized approach is shown in Figure 10. It can be seen that there is an excellent agreement between MSG and DNS predictions for displacement, $\overline{u}_3$. However, there was a significant loss of accuracy when the displacement field was predicted using the homogenized approach.

Figure 11 presents the local stress distribution of σ_{11} and σ_{22} along the thickness direction. The stress distribution was plotted at $x_1 = 1.575$ mm, $x_2 = 0.075$ mm, $x_3 = 0 - 0.07$ mm. The plots show that there is an excellent

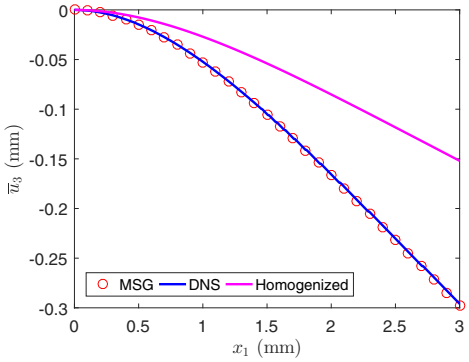

Figure 10. Deflection, $\overline{u}_3$, in 3D orthogonal beam along x_1 direction

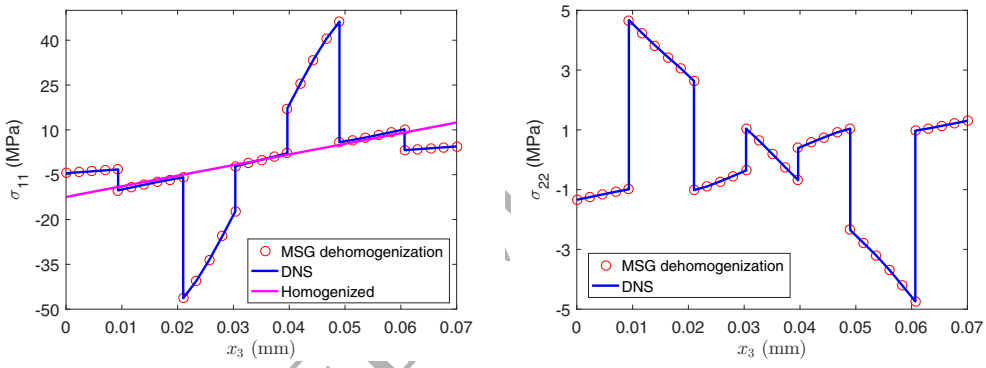

(a) σ_{11} (b) σ_{22}

Figure 11. Stress distribution in 3D orthogonal beam through the thickness based on different models

agreement among stress distributions of σ_{11} and σ_{22} obtained from MSG and DNS. Overall, MSG predicted all stress variations and discontinuities along the thickness direction. However, like for the plain weave beam structure, the homogenized approach could only capture σ_{11} with linear stress distribution. The homogenized approach could not capture the discontinuities and shifts in the local stress fields of σ_{11} and the max stresses predicted are very different

from the exact stresses in the original structure predicted by DNS.

In terms of efficiency, DNS took five hours and 56 minutes with 20 CPUs to complete the analysis. For MSG, it took one hour and 58 minutes with one CPU for the entire analysis.

4.4. Plain weave composite plate

In this example, multiscale structural analysis of a plain weave plate-like textile structure is performed using MSG and compared with other approaches. This structure consists of two plies of plain weave fabric having thickness equal to 0.02 mm each. The length and width are equal to 2.1 mm. The 3D SG for this plain weave plate-like textile structure is the same as for the plain weave beam-like textile structure. 3D SG and original the plain weave structure are shown in Figure 12.

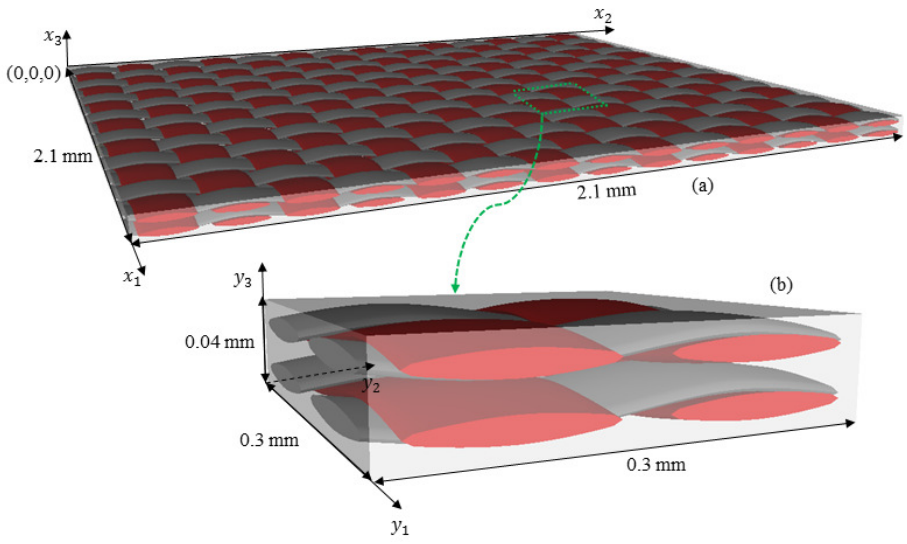

Figure 12. Plain weave composite plate and its SG: a) 3D plain weave structure; b) 3D plate SG

The non-zero components of the plate stiffness matrix $A_{11} = 1.57 \times 10^3\,\mathrm{N/mm}$, $A_{22} = 1.57 \times 10^3\,\mathrm{N/mm}$, $A_{12} = A_{21} = 2.25 \times 10^2\,\mathrm{N/mm}$, $A_{66} = 1.09 \times 10^2\,\mathrm{N/mm}$, $D_{11} = 1.89 \times 10^{-1}\,\mathrm{N \cdot mm}$, $D_{22} = 1.89 \times 10^{-1}\,\mathrm{N \cdot mm}$, $D_{12} = D_{21} = 1.45 \times 10^{-2}\,\mathrm{N \cdot mm}$, $D_{66} = 1.43 \times 10^{-2}\,\mathrm{N \cdot mm}$ were used as an input for the 2D macroscopic plate analysis. The length and width of the 2D model were equal to 2.1 mm each. Plate was clamped at one end and the other end was free. The uniform pressure of magnitude 10^{-2} MPa along negative x_3 direction was applied. This analysis outputs global plate strains and curvatures (Eq. (14)), which were used as inputs to perform the MSG-based dehomogenization analysis to recover local stress and strain fields.

MSG-based global displacement and local stress fields of plain weave plate-like structure were compared with those of DNS to verify the accuracy of MSG-based approach. DNS of the original structure was conducted in Abaqus 6.13. This 3D structure was discretized using 4,233,600 20-noded brick elements. Fixed-free boundary conditions were applied to the 3D textile structure.

Like for the previous two examples, global displacement and stress fields for the plain weave plate-like structure were also predicted by using the homogenized approach. Material stiffness matrix for this case was the same as for the plain weave textile-beam like structure. Plate was modelled in 2D space having length and width equal to 2.1 mm×2.1 mm each. Shell thickness was kept to be 0.04 mm. Boundary conditions and mesh was kept the same as for MSG-based approach for the plain weave plate-like structure.

The displacement, $\overline{u}_3$, results for three approaches are presented in Figure 13. MSG-based predicted displacement field matched exactly with that

of DNS. However, homogenized approach predicted smaller values for the displacement field as compared to the MSG and DNS approach.

The stress distributions of σ_{11}, σ_{22}, and σ_{33} along the thickness direction are presented in Figure 14. This distribution was plotted through the thickness at $x_1 = 1.275$ mm, $x_2 = 1.275$ mm, $x_3 = 0 - 0.04$ mm. MSG-based stress distributions match exactly with those of DNS. MSG not only captured the variations in stresses, but it also predicts the discontinuities in the stresses accurately. It is clear that MSG accurately predicts stress distributions of σ_{11}, σ_{22}, and σ_{33} in plain weave plate-like structures. However, the homogenized approach captured σ_{11} with linear distribution through the thickness which is very different from the actual stress distributions in the original heterogeneous structures. Additionally, homogenized approach predicted σ_{22} negligibly small as compared to the ones predicted by MSG and DNS and the homogenized approach cannot predict a nonzero value for σ_{33}.

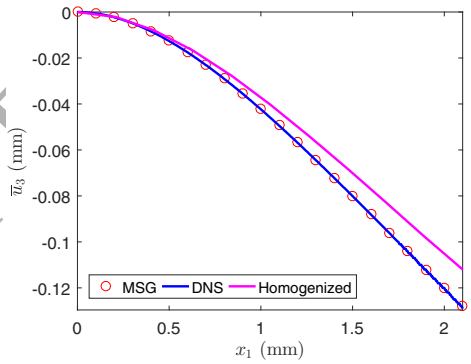

Figure 13. Deflection, $\overline{u}_3$, in plain weave plate along x_1 direction

In terms of the computing efficiency, MSG-based analysis took only two hours and 16 minutes with one CPU for the entire analysis. However, DNS

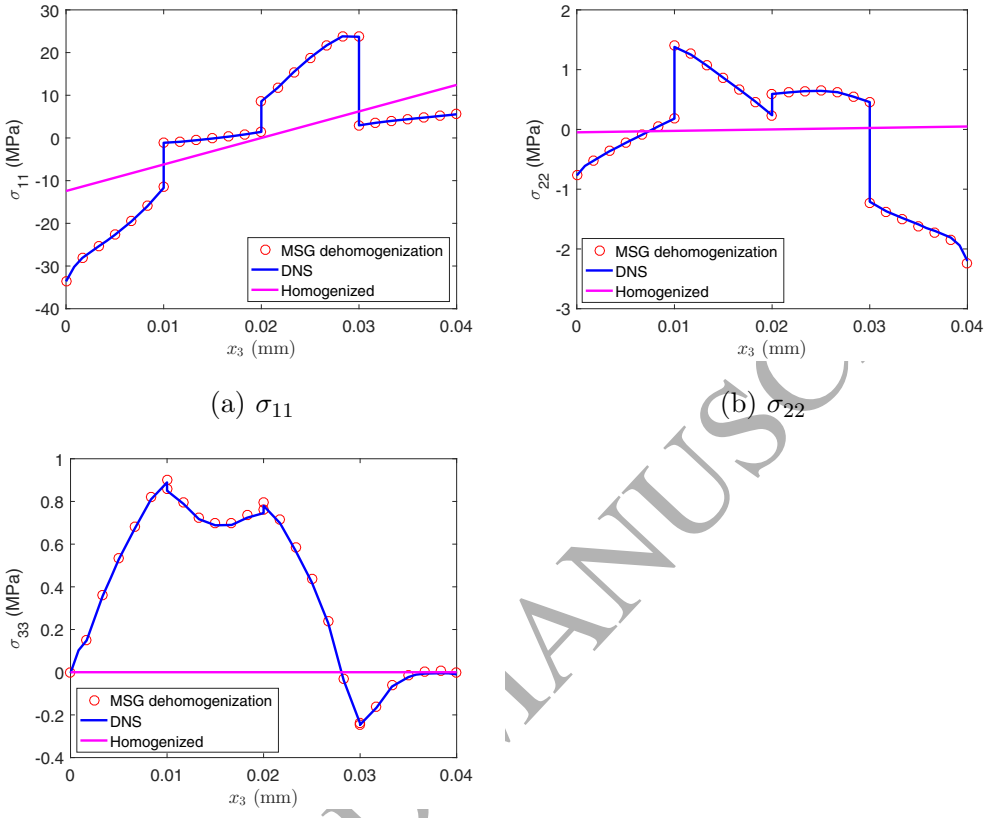

(a) σ_{11} (b) σ_{22}

(c) σ_{33}

Figure 14. Stress distribution in plain weave plate through the thickness based on different models

took eight hours and four minutes with 60 CPUs.

4.5. 3D orthogonal textile plate

In this example, multiscale modeling of a 3D orthogonal plate-like structure was conducted using MSG, DNS and the homogenized approach. The length, width, and thickness of the original structure were 3 mm, 3.6 mm and 0.07 mm respectively. 3D SG was the same as for 3D orthogonal beam-like

textile structures as shown in Figure 15.

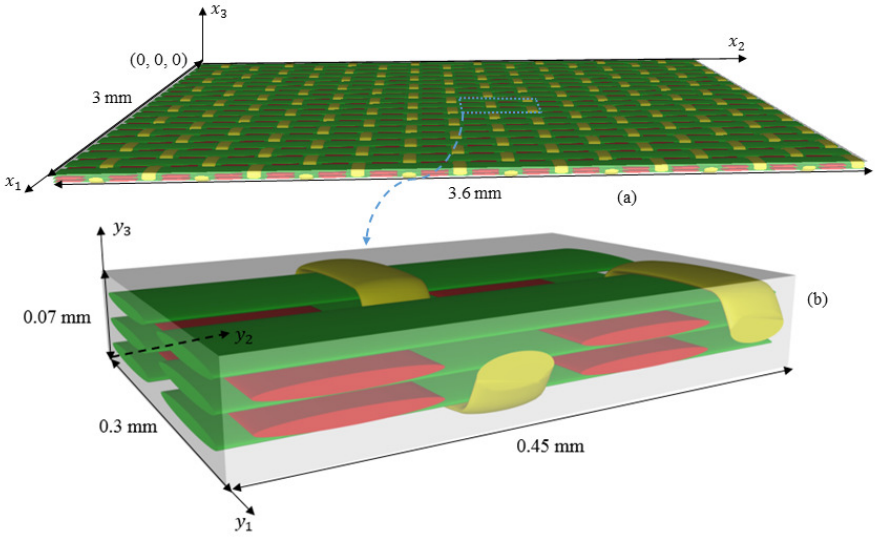

Figure 15. 3D orthogonal composite structure and its SG: a) 3D Orthogonal structure; b) 3D plate SG

The 2D plate analysis was conducted in Abaqus 6.13. Then non-zero terms of MSG predicted plate stiffness matrix $A_{11} = 1.60 \times 10^3$ N/mm, $A_{22} = 2.82 \times 10^3$ N/mm, $A_{12} = A_{21} = 1.95 \times 10^2$ N/mm, $A_{66} = 1.69 \times 10^2$ N/mm, $D_{11} = 3.49 \times 10^{-1}$ N $\cdot$ mm, $D_{22} = 8.08 \times 10^{-1}$ N $\cdot$ mm, $D_{12} = D_{21} = 6.93 \times 10^{-2}$ N $\cdot$ mm, $D_{66} = 6.12 \times 10^{-2}$ N $\cdot$ mm were used as an input. Fixed-free boundary conditions were applied to the plate, and the plate was subjected to a uniform pressure of 10^{-2} MPa along negative x_3 direction. This analysis outputs global responses (the strains and curvatures), which were extracted at $x_1 = 1.575$ mm, $x_2 = 1.875$ mm point. The responses were used as inputs for the dehomogenization analysis.

DNS of the original 3D orthogonal structure was conducted in Abaqus 6.13. This 3D structure was discretized using 5,760,000 20-noded brick elements. The boundary conditions and load were kept the same as for the plain weave plate-like textile structure.

Global displacement and local stess field results for the 3D orthogonal structure were also predicted by using the homogenized approach. Effective stiffness matrix was the same as for the 3D orthogonal textile-beam like structure. Plate was modelled as 2D plane having length and width equal to 3 mm $\times$ 3.6 mm each. Plate thickness was kept equal to 0.07 mm. Boundary conditions, loading and mesh was kept the same as for MSG-based approach for the 3D orthogonal plate-like structure.

The displacement, $\overline{u}_3$, results for three approaches are presented in Figure 16. MSG-based displacement field match exactly with that of DNS. However, there was significant loss of accuracy when the displacement field was predicted using the homogenized approach.

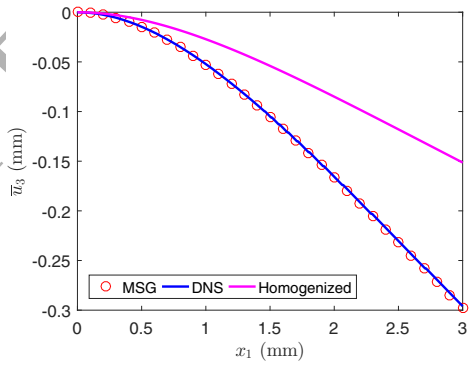

Figure 16. Deflection, $\overline{u}_3$, in 3D orthogonal plate along x_1 direction

Figure 17 presents the stress distribution of σ_{11} and σ_{22} for MSG and

DNS. This distribution was taken at $x_1 = 1.575$ mm, $x_2 = 1.875$ mm, $x_3 = 0 - 0.07$ mm. MSG captured in-plane normal stress components (σ_{11}, σ_{22}) with the same accuracy as DNS. Based on the results, it is clear that MSG is fully capable of predicting the deflection and stress distributions of complicated plate-like 3D orthogonal textile structures. Like in the previous example, the homogenized approach could not accurately capture the local stress fields.

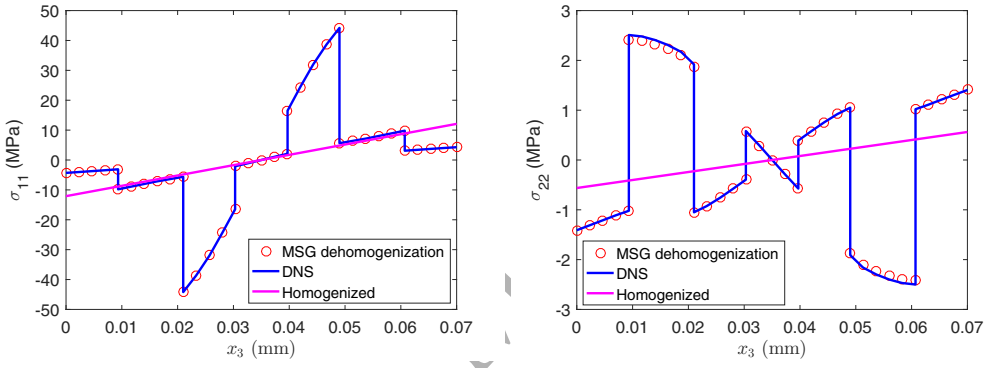

(a) σ_{11} (b) σ_{22}

Figure 17. Stress distribution in 3D orthogonal plate through the thickness based on different models

In terms of efficiency, MSG-based analysis took approximately two hours and three minutes with one CPU for the entire analysis. However, DNS took twenty hours and two minutes with 80 CPUs.

4.6. Discussion

Based on the beam and plate examples shown in this section, it is clear that MSG beam and plate models can predict the global structural displacements and local stress fields with almost the same accuracy as 3D DNS

approach, while the computing time for MSG beam and plate models is significantly lower than that for DNS. In other words, MSG beam and plate model provides an accurate and efficient way to analyze textile beam and plate structures. Because different types of textile composites can be discretized using finite element meshes and then analyzed using the MSG-based multiscale modeling framework, MSG beam and plate models are not restricted to a certain type of textiles, they can be used to analyze general textile composites having simple or complicated architectures.

From the deflection results, it is clear that homogenized approach predicted smaller deflection values than the other two approaches. If a structure is designed based on the homogenized approach, it may be unsafe because the real deflection will be larger than the one predicted by the homogenized approach. The stresses obtained using homogenized approach are taken at macro-structural level. Usually, it is difficult to recover the local stresses in the MSG solid model as well as in the RVE with the structural responses coming from beam and plate elements. Therefore, if the stresses at macro-structural level are taken as a design parameter, there will be a great loss of accuracy as shown in the above examples. However, MSG beam and plate models can easily recover the local fields with all the stress components based on the structural responses using common beam and plate elements available in any commercial FEA software. It is important to note that the inaccurate results computed by the homogenized approach using the MSG solid model doesn't mean the MSG solid model is not accurate. The main reason is that the beam and plate structures usually doesn't meet the periodicity requirements in all directions, while the effective properties used in homogenized

properties are obtained for the structures featuring 3D periodicity. In other words, if a structure has 3D periodicity and needs to be modelled using solid elements, then the MSG solid model should be used in that case.

5. Conclusion

MSG is extended to provide a novel multiscale structural modeling approach for textile composite structures. This approach combines homogenization, structural analysis and dehomogenization, which decouples the original complex structural analysis to constitutive modeling and macroscopic beam and plate analysis. For MSG homogenization, yarn homogenization is performed first based on the properties of fiber and matrix. It is demonstrated by examples that MSG has the capability to predict the homogenized response of yarns having realistic shapes and many fibers. Plate and beam stiffness matrices are computed directly in terms of yarn and matrix properties. Based on these stiffness matrices, 1D beam and 2D plate structural analyses are conducted to predict the global responses. Finally, 3D stress fields are recovered using MSG-based dehomogenization approach. The global displacements and local stress distributions are compared with DNS for four different textile structures (2 textile beams and 2 textile plates). An excellent agreement among the results was observed. In addition to that, computational costs of MSG-based approach are significantly lower than DNS. It is also shown that homogenized approach does not provide accurate prediction of displacement and stress fields for slender and thin textile structures. However, the homogenized approach will take similar time as the MSG-based beam/plate analysis. Therefore, it is better to use beam and plate constitutive relations

to perform beam and plate structural analysis instead of using homogenized material properties. MSG provides a unified and rigorous way to predict the beam and plate constitutive relations based on the SG of the textile composites, which can be directly used in the structural analysis in most commercial FEA codes. Based on this research work, it can be confidently said that MSG can be used to perform multiscale structural analysis of textile composites at much lower computing costs and maintains almost the same accuracy as of DNS of the original heterogeneous model. This novel approach can be confidently used in designing structures made from complicated textile composites with much less modeling efforts and computing time than DNS.

Acknowledgement

The authors gratefully appreciate the TexGen developers for providing the open source codes. We also thank Composites Design and Manufacturing HUB (cdmHUB.org) to provide the cloud platform so that users can easily use the available tools.

Appendix A. plate and beam stiffness matrix

The 3D strain field for MSG beam and plate models can be expressed in a unified form

$$\Gamma = \Gamma_h w + \Gamma_\epsilon \bar{\epsilon} \tag{A.1}$$

where $\Gamma = [\varepsilon_{11} \quad \varepsilon_{22} \quad \varepsilon_{33} \quad \varepsilon_{23} \quad \varepsilon_{13} \quad \varepsilon_{12}]$ represents the 3D strain field of the original structure. Γ_h is an operator matrix which depends on the dimensionality of the SG. Γ_ϵ is an operator matrix which depends on the macroscopic structural model. The detailed expressions for the operator matrices can be

found in [13]. For the beam model, $\bar{\epsilon}$ is the beam strain measures in Eq. (6). For the plate model, $\bar{\epsilon}$ is the plate strain measures in Eq. (14). The strain energy density can be expressed as

$$U = \left\langle \left(\Gamma_h w + \Gamma_\epsilon \bar{\epsilon}\right)^T C \left(\Gamma_h w + \Gamma_\epsilon \bar{\epsilon}\right) \right\rangle \tag{A.2}$$

MSG uses a finite element mesh to discrete the analysis domain, and the fluctuating functions can be expressed using shape functions defined over SG as

$$w\left(x_k, y_j\right) = S(y_j) V(x_k) \tag{A.3}$$

where V is what we need to solve for as the nodal values for the fluctuating function based on the discretization. Substituting Eq.(A.3) into Eq. (A.2),

$$U = \frac{1}{2}\left(V^T E V + 2V^T D_{h\epsilon}\bar{\epsilon} + \bar{\epsilon}^T D_{\epsilon\epsilon}\bar{\epsilon}\right) \tag{A.4}$$

where

$$E = \left\langle (\Gamma_h S)^T C (\Gamma_h S) \right\rangle, D_{h\epsilon} = \left\langle (\Gamma_h S)^T C \Gamma_\epsilon \right\rangle, D_{\epsilon\epsilon} = \left\langle \Gamma_\epsilon^T C \Gamma_\epsilon \right\rangle \tag{A.5}$$

Solving V, we can get the strain energy in the SG as

$$U = \frac{1}{2}\left(\bar{\epsilon}^T (V_0^T D_{h\epsilon} + D_{\epsilon\epsilon})\bar{\epsilon}\right) \equiv \frac{\omega}{2}\bar{\epsilon}^T \bar{C} \bar{\epsilon} \tag{A.6}$$

where $\bar{C}$ is the effective stiffness to be used in the macroscopic structural model and ω is the volume of the SG. For the beam model used in this paper, $\bar{C}$ is the 4×4 stiffness matrix in Eq. (11). For the plate model used in this paper, $\bar{C}$ is the 6×6 stiffness matrix in Eq. (19). The effective stiffness can be used as inputs for the structural analysis to obtain the global strains $\bar{\epsilon}$ which can be used in Eq. (A.1) to obtain the local strain field, which can be further used to obtain the local stress field using Hooke's law.

References

[1] B. V. Sankar, R. V. Marrey, Analytical method for micromechanics of textile composites, Composites Science and Technology 57 (6) (1997) 703–713.

[2] K. Bilisik, Dimensional stability of multiaxis 3D-woven carbon preforms, The Journal of The Textile Institute 101 (5) (2010) 380–388.

[3] X. Liu, K. Rouf, B. Peng, W. Yu, Two-step homogenization of textile composites using mechanics of structure genome, Composite Structures 171 (2017) 252–262.

[4] X.-Y. Zhou, P. Gosling, C. Pearce, Z. Ullah, L. Kaczmarczyk, Perturbation-based stochastic multi-scale computational homogenization method for woven textile composites, International Journal of Solids and Structures 80 (2016) 368–380.

[5] E. J. Barbero, T. M. Damiani, J. Trovillion, Micromechanics of fabric reinforced composites with periodic microstructure, International Journal of Solids and Structures 42 (9) (2005) 2489–2504.

[6] B. V. Sankar, R. V. Marrey, A unit-cell model of textile composite beams for predicting stiffness properties, Composites Science and Technology 49 (1) (1993) 61–69.

[7] T. Ishikawa, T.-W. Chou, Stiffness and strength behaviour of woven fabric composites, Journal of Materials Science 17 (11) (1982) 3211–3220.

[8] T.-W. Chou, T. Ishikawa, One-dimensional micromechanical analysis of woven fabric composites, AIAA Journal 21 (12) (1983) 1714–1721.

[9] T. Ishikawa, Anti-symmetric elastic properties of composite plates of satin weave cloth, Fibre Science and Technology 15 (2) (1981) 127–145.

[10] J.-M. Yang, C.-L. Ma, T.-W. Chou, Fiber inclination model of three-dimensional textile structural composites, Journal of Composite Materials 20 (5) (1986) 472–484.

[11] P. Chaphalkar, A. D. Kelkar, Classical laminate theory model for twill weave fabric composites, Composites Part A: Applied Science and Manufacturing 32 (9) (2001) 1281–1289.

[12] R. V. Marrey, B. V. Sankar, A micromechanical model for textile composite plates, Journal of Composite Materials 31 (12) (1997) 1187–1213.

[13] W. Yu, A unified theory for constitutive modeling of composites, Journal of Mechanics of Materials and Structures 11 (4) (2016) 379–411.

[14] X. Liu, W. Yu, A novel approach to analyze beam-like composite structures using mechanics of structure genome, Advances in Engineering Software 100 (2016) 238–251.

[15] B. Zhao, Analysis of composite plates by using mechanics of structure genome, Master's thesis, Purdue University West Lafayette, 2016.

[16] N. Liu, W. Yu, Evaluation of Smeared Properties Approaches and Mechanics of Structure Genome for Analyzing Composite Beams, Mechanics of Advanced Materials and Structures (just-accepted).

[17] B. Peng, J. Goodsell, R. B. Pipes, W. Yu, Generalized free-edge stress analysis using mechanics of structure genome, Journal of Applied Mechanics 83 (10) (2016) 101013.

[18] H. Lin, L. P. Brown, A. C. Long, Modelling and simulating textile structures using TexGen, in: Advanced Materials Research, vol. 331, Trans Tech Publ, 44–47, 2011.

[19] A. Bensoussan, J.-L. Lions, G. Papanicolaou, Asymptotic analysis for periodic structures, Studies in Mathematics and its Applications 5, North-Holland Publishing Company Amsterdam, 1978.

[20] V. Berdichevsky, Variational principles of continuum mechanics: I. Fundamentals, Berlin: Springer Science & Business Media, 2009.

[21] K. Kirane, M. Salviato, Z. P. Bažant, Microplane triad model for simple and accurate prediction of orthotropic elastic constants of woven fabric composites, Journal of Composite Materials 50 (9) (2016) 1247–1260.

[22] J. Zeman, M. Šejnoha, Numerical evaluation of effective elastic properties of graphite fiber tow impregnated by polymer matrix, Journal of the Mechanics and Physics of Solids 49 (1) (2001) 69–90.